Research Square

Preprints are preliminary reports that have not undergone peer review.
They should not be considered conclusive, used to inform clinical practice,
or referenced by the media as validated information.

Deep lower-mantle water reservoir implied by the stability of a mixed-valence hydrous iron-rich oxide

Lu Liu
Center for High Pressure Science and Technology
Ziqiang Yang
Center for High Pressure Science and Technology
Hongsheng Yuan
Center for High Pressure Science and Technology
Yue Meng
Carnegie Institute of Washington
Nico Giordano
Deutsches Elektronen-Synchrotron
Junliang Sun
Peking University https://orcid.org/0000-0003-4074-0962
Xueyan Du
Center for High Pressure Science and Technology Advanced Research
Philip Dalladay-Simpson
Center for High Pressure Science & Technology Advanced Research https://orcid.org/0000-0002-6213-4472
Junyue Wang
Center for High Pressure Science and Technology Advanced Research
Li Zhang (zhangli@hpstar.ac.cn)
Center for High Pressure Science and Technology

Article

Keywords: petrology, lower mantle

Posted Date: January 13th, 2021

DOI: https://doi.org/10.21203/rs.3.rs-138240/v1

License: This work is licensed under a Creative Commons Attribution 4.0 International License.
Read Full License

Abstract

The lower mantle, containing both primordial and recycled water, is the most massive potential water reservoir in the Earth. Geophysical and geochemical evidence combined have suggested that the largest heterogeneities in the deep lower mantle may serve as primitive deep-mantle reservoirs hosting a variety of incompatible species including hydrogen. To understand water storage in the deep lower mantle, we conducted experiments in the Fe-O-H, Fe-Al-O-H and Fe-Al-Mg-Si-O-H systems under high pressure-temperature (P-T) conditions, and discovered a previously unknown hexagonal phase (referred to as “H1-phase”) in all the systems. The single-crystal structure of the H1-phase was determined at 79 GPa with a unit-cell of a=10.022(2)Å and c=2.6121(9) Å and the space group of P63/m, and its composition was obtained as Fe12.76O18H3.7 combining the structure determination and chemical analysis on the recovered sample. More importantly, about 20 mol% of MgO, Al2O3 and SiO2 can be incorporated into the H1-phase in a realistic mantle system Fe-Al-Mg-Si-O-H and its stability field is extended to at least 2400 km along a normal geotherm, implying that the H1-phase can store primordial water in the deepest lower mantle. Therefore, plume-generation zones originated from the deepest lower mantle provide a potential source for higher water contents in basalts associated with mantle plume components.

Introduction

The lower mantle, containing both primordial and recycled water [1], is the most massive potential water reservoir in the Earth. Geophysical and geochemical evidence combined have suggested that the largest heterogeneities in the deep lower mantle may serve as primitive deep-mantle reservoirs hosting a variety of incompatible species including hydrogen [2, 3]. To understand water storage in the deep lower mantle, we conducted experiments in the Fe-O-H, Fe-Al-O-H and Fe-Al-Mg-Si-O-H systems under high pressure-temperature (*P-T*) conditions, and discovered a previously unknown hexagonal phase (referred to as “H1-phase”) in all the systems. The single-crystal structure of the H1-phase was determined at 79 GPa with a unit-cell of *a*=10.022(2)Å and *c*=2.6121(9) Å and the space group of *P63/m*, and its composition was obtained as $Fe_{12.76}O_{18}H_{3.7}$ combining the structure determination and chemical analysis on the recovered sample. More importantly, about 20 mol% of MgO, Al_2O_3 and SiO_2 can be incorporated into the H1-phase in a realistic mantle system Fe-Al-Mg-Si-O-H and its stability field is extended to at least 2400 km along a normal geotherm, implying that the H1-phase can store primordial water in the deepest lower mantle. Therefore, plume-generation zones originated from the deepest lower mantle provide a potential source for higher water contents in basalts associated with mantle plume components [1, 4].

Global tomography revealed the Pacific and African superplumes in the lower 1000 km of the mantle [5, 6]. Combined evidence from geophysics, geochemical and dynamic calculations have suggested that the superplumes are dense and have a chemical origin [7, 8, 9]. The origin of the chemical heterogeneities is still an area of active debate. Formation of a deep magma body early in the Earth’s history would be expected to concentrate a variety of incompatible species including hydrogen in the deepest heterogeneities [2, 4]. The sites of both large igneous province (LIP) eruption and active hotspot volcanoes lie vertically above

the edges of the African and Pacific superplumes [10]201, implying a possible lower mantle source for the primordial noble gases and higher water contents in basalts associated with mantle plume components [1, 3, 11]. Characterization of the volatile contents of different mantle components indicates that recycled oceanic crust is efficiently dehydrated during subduction and therefore water in ocean island basalts is a combination of primordial and recycled water [1]. Recent calculations suggested that water would preferentially partition into the iron liquid at the core mantle boundary [12]. Despite large uncertainties in the budget and distribution of water in the Earth, water, even in extremely small amounts, can significantly affect mantle phase equilibrium and play a critical role in mantle dynamics [13].

Phase equilibrium data on water-bearing multicomponent systems under the extreme high pressure-temperature (*P-T*) conditions can provide constraints on water storge and effects of water on the phase relations in a lower mantle system. The water solubility in bridgmanite, the dominant mineral in the lower mantle, remains a debated issue [14, 15]. The dense hydrous magnesium silicates (DHMS phases), phase D [$MgSi_2H_2O_6$] and phase H [$MgSiO_4H_2$], may transport water into the lower mantle through subduction [16, 17]. Experimental data on the Al-bearing multicomponent systems have showed that the thermal stability of the phase H is greatly enhanced by incorporation of alumina under *P-T* conditions throughout the lower mantle [17, 18, 19, 20]. The phase H, δ-AlOOH, ε-FeOOH and $CaCl_2$-type SiO_2 all adopt the similar orthorhombic structure under the *P-T* conditions of the lower mantle except that ε-FeOOH transforms to a cubic pyrite-structured $FeOOH_x$ ($0<x\leq1$) (referred to as “py-phase”) above 85 GPa [21, 22]. Recent preliminary experiments in the MgO-Al_2O_3-Fe_2O_3-SiO_2-H_2O system indicate that a considerable amount of FeOOH can still be incorporated into the solid solutions of phase H and δ-AlOOH above 85 GPa [23]. For simplicity, we refer to all solid solutions between phase H, d-AlOOH and e-FeOOH as the δ-phase.

Iron (Fe) is the most abundant transition metal in the mantle and the dominant element in the core. Iron reacts with water to form wüstite (FeO) and iron hydride (FeH) when iron is over saturated in the system [24, 25]. The run products would be different depending on water availability in a Fe-O-H system [25]. Overall, the phase equilibria in the Mg-Si-Fe-Al-O-H system are not sufficiently known to understand the effect of pressure and chemical compositions on water storage in Fe-bearing multicomponent hydrous systems under high *P-T* conditions of the deep lower mantle.

There have been few phase equilibrium data in hydrous multicomponent systems mainly due to the difficulties in characterization of coexisting phases in a multiphase assemblage synthesized at extremely high *P-T* conditions. Combining *in-situ* multigrain X-ray diffraction (XRD) with *ex-situ* transmission electron microscopy (TEM) analysis, we are able to determine chemical composition and crystal structure of 100-300 nm individual grains in a multiphase assemblage synthesized at high *P-T* conditions [26, 27]. In this study, we conducted a series of experiments in the Fe-O-H, Fe-Al-O-H and Fe-Al-Mg-Si-O-H systems using a laser-heated diamond anvil cell (LH-DAC) under high *P-T* conditions of the deep lower mantle (Supplementary Table 1), identified a new hexagonal hydrous Fe-rich phase with a mixed valence state, and discussed the water effects on the chemical heterogeneities in the deep lower mantle.

Discovery and characterization of the H1-phase

First, the starting material $Al_{0.2}Fe_{0.8}(OH)_3$ was loaded in a Ne medium (Run# Sa083, Supplementary Table 1). When the sample was heated to 1600 K at 79 GPa, only the diffraction peaks of the orthorhombic δ-phase appeared. When *T* was increased to 1800 K, a new set of peaks appeared in addition to those of the δ-phase. We observed a gradual growth of the new phase at the expense of the δ-phase and it became dominant at 2100 K, with a hexagonal unit-cell of *a*=10.022(2) Å and *c*=2.6121(9) Å at 79 GPa and after *T* quench (referred to as the "H1-phase"), as shown in Fig. 1. The results indicate that the Fe-bearing δ-phase (Fe,Al)OOH is unstable under high *P-T* conditions of the deep lower mantle along a normal geotherm [28].

The H1-phase was reproduced in two separate runs coexisting with the δ-phase using the same starting material $Al_{0.2}Fe_{0.8}$ $(OH)_3$ (Run# Sb211, Sb343a, Supplementary Table 1 and Fig. 1). To identify the chemical composition of the H1-phase, the sample synthesized at 80 GPa and 2100 K (Run Sb #343a) was recovered to ambient conditions for phase identification and chemical analysis by TEM. We found that the Al content in the H1-phase was negligible containing only ~1.5 at.% Al, but the Fe/(Fe+Al) ratio was reduced from 80 at.% in the starting material to ~13 at.% in the δ-phase (Supplementary Fig. 2). As shown by the contrast between the coexisting H1-phase and δ-phase (Fe,Al)OOH in the elemental mapping of oxygen, the H1-phase contains slightly less oxygen content than (Fe,Al)OOH. However, the exact oxygen content in the H1-phase cannot be determined by chemical analysis on the recovered sample due to the presence of residual water in the system. When the *P-T* conditions were increased to 86 GPa and 2300 K, we found that the H1-phase coexisted with the δ-phase and the py-phase (Run# Sb069), indicating that the H1-phase is a low-pressure phase relative to the py-phase.

The H1-phase was again successfully synthesized in the Fe-O-H system with the starting material $Fe(OH)_3$ (equivalent to Fe_2O_3+3H_2O) in a Ne medium at 78 GPa and 2000 K (Run# Sb343b). A nearly pure H1-phase was again obtained with *a*=10.014(2) Å and *c*=2.6158(6) Å coexisting with a small amount of *ε*-FeOOH. The sample was further heated at 2200 K for another 10 minutes to test its thermal stability and the H1-phase remained stable only with better crystallization (Fig. 2A).

The Earth's mantle contains both ferric and ferrous iron. For comparison, we conducted another experiment on FeO loaded in a saturated water medium. The sample was compressed to 80 GPa and then heated at 2100 K for 10 minutes (Run# Sb390) and the H1-phase was again obtained coexisting with ice-VII (Fig. 2B), indicating that formation of the H1-phase is independent of the valence state of iron in a hydrous deep lower mantle. The H1-phase was slowly decompressed and the XRD pattern was collected immediately after decompression to ambient conditions, showing only weak peaks of the H1-phase, and the unit-cell parameters of *a*=11.437(3) Å, *c*=2.9285(14) Å and *V*=331.8(2) $Å^3$ were obtained at ambient conditions. The diffraction signal of the H1-phase gradually disappeared with time under ambient conditions (Supplementary Fig. 3).

Determination of the chemical composition and crystal structure of the H1-phase is a challenge due to its unquenchable crystal structure. Fortunately, spottiness of the XRD pattern of the H1-phase in the Fe-Al-O-H system (Run# Sa083) allows in-situ multigrain indexation and single-crystal structure determination [27, 29]. The structural information can be used to constrain its chemical formula because the H1-phase contains mainly Fe and O where the Al content (~1.5 at.%) is negligible. Hydrogen is undetectable by XRD if present. The sample was aligned to the rotation center and a dataset was collected by rotating the DAC from -26.0 to 25.0° in small incremental steps of 0.25°. The X-ray wavelength was 0.3445 Å and the exposure time was 5s/frame. Through the determination of crystallographic orientations for individual grains [30], we indexed 28 individual grains belonging to the H1-phase, and three of the grains were selected for further structure determination and refinement. The XDS package was used for single-crystal data reduction [31]. In total 774 reflections have been merged from the three grains. A reasonable *R1* = 5.59% was obtained for all data. The reflections obtained from the powder XRD and the refined atomic coordinates determined from the single-crystal structure are given in Table 1 and the structure and refinement details is provided in the supplementary CIF. The chemical formula of the H1-phase was obtained as $Fe_{12.76}O_{18}H_x$ with O/Fe=1.41 less than O/(Fe+Al)=2.0 in the coexisting δ-phase consistent with the O mapping (Supplementary Fig. 2). Assuming a linear relationship between the density of iron oxides and the O/Fe ratio at 78 GPa, the measured density of the H1-phase assuming a composition of $Fe_{12.76}O_{18}$ is ~3.3% smaller than the calculated value, suggesting that the H1-phase contains a considerable amount of H (details see the supplementary Note 6). The volume expansion induced by incorporation of hydrogen into the lattice was determined as ~2.0 $Å^3$ per hydrogen atom based on the neutron diffraction data of $ReH_{0.23}$ [32]. The H content was then derived as x~3.7 in the H1-phase as $Fe_{12.76}O_{18}H_{3.7}$.

The H1-phase has a similar unit-cell with the recently reported OE-phase [33] and η-phase [34], but both the studies suggest a molar ratio of O/Fe>1.5 with a chemical formula of $(Mg,Fe)_2O_{3+\delta}$ ($0 < \delta < 1$) [33] or $Fe_{12}O_{18+x/2}H_x$ ($x \approx 2$) [34], respectively. On the contrary, we obtained $Fe_{12.76}O_{18}H_{3.7}$ with O/Fe<1.5 from our single-crystal structure data. The discrepancy originates from whether the hexagonal channels formed with chains of FeO_6 octahedra is occupied by Fe or O. In our analysis, the electron density peak of the position and structural refinement clearly indicated partially occupied Fe with a site occupation factor (SOF) =0.381 instead of O. Furthermore, strong Raman signal of O_2 was detected in the sample chamber where $Fe(OH)_3$ was used as the starting material (Run# Sb343b) and the run product was a nearly pure H1-phase (Supplementary Fig. 4 and Fig. 2A), confirming the O_2 release during the formation of H1-phase from a starting material all in Fe^{3+}. Combined evidence from single-crystal XRD determination and Raman spectroscopy indicates that the H1-phase is a mixed-valence hydrous iron oxide with nearly equal amount of Fe^{2+} and Fe^{3+}. A series of mixed-valence iron oxides have been discovered at high pressures and temperatures [35, 36]. However, whether a mixed-valence hydrous iron oxide is stable in the lower mantle requires further investigation in a realistic multicomponent composition.

Water storage in the deep lower mantle

We performed an experiment on a hydrous gel of 40 mol% $MgSiO_3$-30 mol% Al_2O_3-30 mol% Fe_2O_3 containing ~7wt.% H_2O (MASFH30). To better characterize the possible iron oxide and hydrous iron oxide in the assemblage, we used a higher Fe content than that in a mid-ocean ridge basalt (MORB) composition [37]. The sample was loaded in a Ne medium (Run# Sb335, Supplementary Table 1) and compressed to 78 GPa and heated at 2000 K for 10 minutes. As shown in Fig. 3A, the diffraction peaks from the multiple phases overlap heavily in the powder XRD pattern where several characteristic peaks of the H1-phase were visible but weak in intensity. To identify the H1-phase and other coexisting phases in the multiphase assemblage, we applied the multigrain method [27] and successfully indexed multiple individual grains belonging to the H1-phase, post-perovskite (pPv) structured Fe_2O_3 phase, bridgmanite (bdg), and the δ-phase, respectively. Supplementary Table 2 provides a list of the reflections from selected grains for each phase in the assemblage and their unit-cell parameters were obtained accordingly. Single-crystal XRD of individual grains contains three-dimensional orientation and geometrical relationship in addition to *d*-spacings and thus the existence of the H1-phase in the assemblage was unambiguously confirmed. The sample was recovered to ambient conditions and the coexisting phases and element distribution are shown in the TEM-EDS images. We observed that a significant amount of Al_2O_3, MgO and SiO_2 can be incorporated into the H1-phase containing about 11.2 at.% Si, 8.5 at.% Mg, and 1.4 at.% Al (Fig. 4 and Table 2).

In another experiment on 65.6 mol% SiO_2-12.3 mol% Al_2O_3- 16.4 mol% MgO-5.7 mol% Fe_2O_3 (MASFH6, Run# Sb307b) that is similar to a simplified MORB composition, the H1-phase was again obtained at 96 GPa and 2300 K containing about 30 at.% (Mg+Si+Al) (Fig. 3B and Table 2). In contrast to ~1.5 at.% Al in the H1-phase at ~80 GPa, the H1-phase contains ~11.2 at.% Al at 96 GPa (Table 2), implying that the composition of the H1-phase is highly dependent on pressure and possibly mantle compositions. The results suggest that incorporation of Al_2O_3, MgO and SiO_2 into the H1-phase extends its stability field from 86 GPa in Fe-Al-O-H system to at least 96 GPa (~108 GPa after accounting for the thermal pressure) at 2300 K in SiO_2-bearing lower mantle system, corresponding to about 2400 km depth in the deep lower mantle. The H1-phase $(Mg0.63Si1.61Al1.43Fe9.10)O18H3.7$ has an estimated density of 6.862 g/cm^3 at 2400 km depth, relative to 5.32 g/cm^3 of the Preliminary Reference Earth Model (PREM) density [38].

Geophysical and geochemical implications

The preliminary results of this study confirmed the stability of the H1-phase in realistic multicomponent systems over a *P-T* range of 80-108 GPa and 2000-2300 K (after accounting for the thermal pressure). Discoveries from mineral physics support a physicochemical boundary at the depth of 1600-1800 km [39] where a series of phase transitions have been discovered in Fe-bearing minerals [21, 40, 41], consistent with a chemical boundary at the middle of the lower mantle [5, 7, 8, 42, 43]. The H1-phase is another Fe-bearing phase stable under *P-T* conditions of this region and its hydrous nature adds further complexities to the chemical heterogeneities. The stability and chemical composition of the H1-phase $(Mg,Si,Al,Fe)_{12.76}O_{18}H_{3.7}$ implies that it may store primordial water depending on actual chemical composition and water concentration in the deep lower mantle. Further detailed exploration in the Mg-Si-

Fe-Al-O-H systems will be needed to determine the relationship between water storage minerals and chemical composition including its water concentration under high *P-T* conditions of the deep lower mantle.

The mixed valence state in the hydrous H1-phase has important implications for the geophysical and geochemical properties of the deep lower mantle. Addition of water and escape of H_2 to the atmosphere has been regarded as an important oxidation mechanism in the mantle [44, 45, 46] and ferric iron can be produced by water-induced oxidation of ferrous iron at shallow depths [44]. Under the deep lower mantle conditions, however, a different mechanism is indicated in this study when the same mixed-valence hydrous iron oxide H1-phase can be produced from chemical reaction between either FeO or Fe_2O_3 with water, implying that high pressure and high temperature in the deep lower mantle stabilizes the crystal-chemistry of the H1-phase. Geophysical and geochemical evidence combined have suggested that the superplumes located at the base of the lower mantle may serve as primitive deep-mantle reservoirs hosting a variety of incompatible species including hydrogen and have been regarded as the largest heterogeneities in the deep mantle [2, 3, 43]. The edges of these heterogeneities seem to have controlled mantle plumes that have generated LIPs and major hotspot volcanoes [4, 10]. Therefore, plume-generation zones in the deepest lower mantle provide a potential source for high water contents in basalts associated with mantle plume components [1, 47].

Methods

The starting materials Al0.2Fe0.8(OH)3, Al0.8Fe0.2(OH)3, Fe(OH)3 , FeO+H_2O and MgO-Fe2O3-SiO2-Al2O3-H2O gels were used in this study and the details of preparation and characterization of the sample were described elsewhere [23]. Composition and homogeneity of the starting materials were confirmed by a scanning electron microscope (SEM) coupled with an energy dispersive X-ray spectroscopy (EDS) analysis (Supplementary Fig. 6). LH-DAC experiments were performed between 70-108 GPa and 1600 K-2400 K. In most runs, Ne was used as insulation layer and pressure medium to generate quasi-hydrostatic pressure, and its equation of state was used to calibrate pressure [48]. All the sample pressures were measured after *T* quench unless noted otherwise. The thermal pressures are estimated as P_{th}=(*T*-300)*0.0062 (GPa) from a previous study under similar *P-T* conditions [23]. In the Runs Sb390 and Sb347, water was used as pressure medium and pressure was calibrated by the Raman shift of diamond [49].

The in-situ laser-heating coupled with XRD measurements were conducted at High Pressure Collaborative Access Team (HPCAT), 16-ID-B beamline of Advanced Photon Source (APS), Argonne National Laboratory (Argonne, IL) (Runs# Sa083). XRD experiments with ex-situ laser-heating were conducted at 15UI beamline of Shanghai Synchrotron Radiation Facility (SSRF) (Runs# Sb211, Sa069, Sb343a, Sb343b, Sb307a, Sb390) and the P02.2 beamline of the PETRA III synchrotron at Deutsches Elektronen Synchrotron (DESY) (Run# Sb335, Sb307b and Sb347). The thin-sections of the recovered samples were prepared using a focused ion beam (FIB). Chemical analysis of recovered samples was performed using

a TEM operating at 200 kV which is equipped with a EDS system. Further details about the experiments and data analysis can be found in the supplementary information (Note 1-5).

Declarations

Acknowledgements

This work was supported from the National Natural Science Foundation of China (NSFC) (Grant No: 41574080). Portions of this work were performed at 15U1, Shanghai Synchrotron Radiation Facility (SSRF). We acknowledge DESY (Hamburg, Germany), a member of the Helmholtz Association HGF, for the provision of experimental facilities. Parts of this research were carried out at the P02.2 beamline of PETRA III. Portions of this work were performed at HPCAT (Sector 16), Advanced Photon Source (APS), Argonne National Laboratory. HPCAT operations are supported by the Department of Energy–National Nuclear Security Administration's (DOE-NNSA's) Office of Experimental Science. The Advanced Photon Source is a U.S. DOE Office of Science User Facility operated for the DOE Office of Science by Argonne National Laboratory un-der contract No. DE-AC02-06CH11357.

References

1. Dixon JE, Leist L, Langmuir C, Schilling J-G. Recycled dehydrated lithosphere observed in plume-influenced mid-ocean-ridge basalt. *Nature* 2002, **420**(6914)**:** 385-389.
2. Labrosse S, Hernlund JW, Coltice N. A crystallizing dense magma ocean at the base of the Earth's mantle. *Nature* 2007, **450**(7171)**:** 866-869.
3. Mukhopadhyay S. Early differentiation and volatile accretion recorded in deep-mantle neon and xenon. *Nature* 2012, **486**(7401)**:** 101-104.
4. Torsvik TH, Burke K, Steinberger B, Webb SJ, Ashwal LD. Diamonds sampled by plumes from the core–mantle boundary. *Nature* 2010, **466**(7304)**:** 352-355.
5. Su W-j, Woodward RL, Dziewonski AM. Degree 12 model of shear velocity heterogeneity in the mantle. *Journal of Geophysical Research: Solid Earth* 1994, **99**(B4)**:** 6945-6980.
6. Ritsema J, Heijst HJv, Woodhouse JH. Complex Shear Wave Velocity Structure Imaged Beneath Africa and Iceland. *Science* 1999, **286**(5446)**:** 1925.
7. Trampert J, Deschamps F, Resovsky J, Yuen D. Probabilistic Tomography Maps Chemical Heterogeneities Throughout the Lower Mantle. *Science* 2004, **306**(5697)**:** 853.
8. Ishii M, Tromp J. Normal-Mode and Free-Air Gravity Constraints on Lateral Variations in Velocity and Density of Earth's Mantle. *Science* 1999, **285**(5431)**:** 1231.
9. Ni S, Tan E, Gurnis M, Helmberger D. Sharp Sides to the African Superplume. *Science* 2002, **296**(5574)**:** 1850.
10. Burke K, Steinberger B, Torsvik TH, Smethurst MA. Plume Generation Zones at the margins of Large Low Shear Velocity Provinces on the core–mantle boundary. *Earth and Planetary Science Letters*

2008, **265**(1)**:** 49-60.

11. Marty B. The origins and concentrations of water, carbon, nitrogen and noble gases on Earth. *Earth and Planetary Science Letters* 2012, **313-314:** 56-66.
12. Li Y, Vočadlo L, Sun T, Brodholt JP. The Earth's core as a reservoir of water. *Nature Geoscience* 2020, **13**(6)**:** 453-458.
13. Iwamori H. Transportation of H2O and melting in subduction zones. *Earth and Planetary Science Letters* 1998, **160**(1-2)**:** 65-80.
14. Fu S, Yang J, Karato S-i, Vasiliev A, Presniakov MY, Gavriliuk AG*, et al.* Water Concentration in Single-Crystal (Al,Fe)-Bearing Bridgmanite Grown From the Hydrous Melt: Implications for Dehydration Melting at the Topmost Lower Mantle. *Geophysical Research Letters* 2019, **46**(17-18)**:** 10346-10357.
15. Litasov K, Ohtani E, Langenhorst F, Yurimoto H, Kubo T, Kondo T. Water solubility in Mg-perovskites and water storage capacity in the lower mantle. *Earth and Planetary Science Letters* 2003, **211**(1)**:** 189-203.
16. Nishi M, Irifune T, Tsuchiya J, Tange Y, Nishihara Y, Fujino K*, et al.* Stability of hydrous silicate at high pressures and water transport to the deep lower mantle. *Nature Geoscience* 2014, **7**(3)**:** 224-227.
17. Pamato MG, Myhill R, Boffa Ballaran T, Frost DJ, Heidelbach F, Miyajima N. Lower-mantle water reservoir implied by the extreme stability of a hydrous aluminosilicate. *Nature Geoscience* 2015, **8**(1)**:** 75-79.
18. Ohira I, Ohtani E, Sakai T, Miyahara M, Hirao N, Ohishi Y*, et al.* Stability of a hydrous δ-phase, AlOOH–MgSiO2 (OH) 2, and a mechanism for water transport into the base of lower mantle. *Earth and Planetary Science Letters* 2014, **401:** 12-17.
19. Walter MJ, Thomson AR, Wang W, Lord OT, Ross J, McMahon SC*, et al.* The stability of hydrous silicates in Earth's lower mantle: Experimental constraints from the systems MgO–SiO2–H2O and MgO–Al2O3–SiO2–H2O. *Chemical Geology* 2015, **418:** 16-29.
20. Sano A, Ohtani E, Kondo T, Hirao N, Sakai T, Sata N*, et al.* Aluminous hydrous mineral δ-AlOOH as a carrier of hydrogen into the core-mantle boundary. *Geophysical Research Letters* 2008, **35**(3).
21. Hu Q, Kim DY, Yang W, Yang L, Meng Y, Zhang L*, et al.* FeO2 and FeOOH under deep lower-mantle conditions and Earth's oxygen–hydrogen cycles. *Nature* 2016, **534**(7606)**:** 241-244
22. Nishi M, Kuwayama Y, Tsuchiya J, Tsuchiya T. The pyrite-type high-pressure form of FeOOH. *Nature* 2017, **547**(7662)**:** 205-208.
23. Yuan H, Zhang L, Ohtani E, Meng Y, Greenberg E, Prakapenka VB. Stability of Fe-bearing hydrous phases and element partitioning in the system MgO–Al2O3–Fe2O3–SiO2–H2O in Earth's lowermost mantle. *Earth and Planetary Science Letters* 2019, **524:** 115714.
24. Ohtani E, Hirao N, Kondo T, Ito M, Kikegawa T. Iron-water reaction at high pressure and temperature, and hydrogen transport into the core. *Physics and Chemistry of Minerals* 2005, **32**(1)**:** 77-82.
25. Nishi M, Kuwayama Y, Hatakeyama T, Kawaguchi S, Hirao N, Ohishi Y*, et al.* Chemical Reaction Between Metallic Iron and a Limited Water Supply Under Pressure: Implications for Water Behavior at

the Core-Mantle Boundary. *Geophysical Research Letters* 2020, **47**(19)**:** e2020GL089616.

26. Zhang L, Popov D, Meng Y, Wang J, Ji C, Li B*, et al.* In-situ crystal structure determination of seifertite SiO2 at 129 GPa: Studying a minor phase near Earth's core–mantle boundary. *American Mineralogist* 2016, **101**(1)**:** 231-234.
27. Zhang L, Yuan H, Meng Y, Mao H-K. Development of High-Pressure Multigrain X-Ray Diffraction for Exploring the Earth's Interior. *Engineering* 2019.
28. Brown JM, Shankland TJ. Thermodynamic parameters in the Earth as determined from seismic profiles. *Geophys J R astr SOC* 1981, **66:** 579-596.
29. Zhang L, Meng Y, Dera P, Yang W, Mao WL, Mao H-k. Single-crystal structure determination of (Mg, Fe) SiO3 postperovskite. *Proceedings of the National Academy of Sciences* 2013, **110**(16)**:** 6292-6295.
30. Sørensen HO, Schmidt S, Wright JP, Vaughan GBM, Techert S, Garman EF*, et al.* Multigrain crystallography. *Zeitschrift für Kristallographie* 2012, **227**(1)**:** 63-78.
31. Kabsch W. XDS. *Acta Crystallographica Section D* 2010, **66**(2)**:** 125-132.
32. Shilstein SS, Glazkov VP, Irodova AV, Somenkov VA, Antonov VE, Ponyatovskii EG. The Crystal Structure of High-Pressure Hydrides. *Zeitschrift für Physikalische Chemie* 1985, **146**(2)**:** 129-135.
33. Liu J, Wang C, Lv C, Su X, Liu Y, Tang R*, et al.* Evidence for oxygenation of Fe-Mg oxides at mid-mantle conditions and the rise of deep oxygen. *National Science Review* 2020.
34. Chen H, Xie S-Y, Ko B, Kim T, Nisr C, Prakapenka V*, et al.* A new hydrous iron oxide phase stable at mid-mantle pressures. *Earth and Planetary Science Letters* 2020, **550:** 116551.
35. Lavina B, Dera P, Kim E, Meng Y, Downs RT, Weck PF*, et al.* Discovery of the recoverable high-pressure iron oxide Fe4O5. *Proceedings of the National Academy of Sciences* 2011, **108**(42)**:** 17281.
36. Bykova E, Dubrovinsky L, Dubrovinskaia N, Bykov M, McCammon C, Ovsyannikov SV*, et al.* Structural complexity of simple Fe2O3 at high pressures and temperatures. *Nature Communications* 2016, **7**(1)**:** 10661.
37. Hirose K, Fei Y. Subsolidus and melting phase relations of basaltic composition in the uppermostlower mantle. *Geochimica et Cosmochimica Acta* 2002, **66**(12)**:** 2099-2108.
38. Dziewonski AM, Anderson DL. Preliminary reference Earth model. *Phys Earth Planet Inter* 1981, **25:** 297-356.
39. Mao H-k, Mao WL. Key problems of the four-dimensional Earth system. *Matter and Radiation at Extremes* 2020, **5**(3)**:** 038102.
40. Badro J, Fiquet G, Guyot F, Rueff J-P, Struzhkin VV, Vankó G*, et al.* Iron Partitioning in Earth's Mantle: Toward a Deep Lower Mantle Discontinuity. *Science* 2003, **300**(5620)**:** 789.
41. Zhang L, Meng Y, Yang W, Wang L, Mao WL, Zeng QS*, et al.* Disproportionation of (Mg,Fe)SiO(3) perovskite in Earth's deep lower mantle. *Science* 2014, **344**(6186)**:** 877-882.
42. van der Hilst RD, Kárason H. Compositional heterogeneity in the bottom 1000 kilometers of Earth's mantle: Toward a hybrid convection model. *Science* 1999, **283**(5409)**:** 1885-1888.

43. Kellogg LH, Hager BH, van der Hilst RD. Compositional Stratification in the Deep Mantle. *Science* 1999, **283**(5409)**:** 1881.
44. Seyfried WE, Foustoukos DI, Fu Q. Redox evolution and mass transfer during serpentinization: An experimental and theoretical study at 200°C, 500bar with implications for ultramafic-hosted hydrothermal systems at Mid-Ocean Ridges. *Geochimica et Cosmochimica Acta* 2007, **71**(15)**:** 3872-3886.
45. Sharp ZD, McCubbin FM, Shearer CK. A hydrogen-based oxidation mechanism relevant to planetary formation. *Earth and Planetary Science Letters* 2013, **380:** 88-97.
46. Elkins-Tanton LT, Grove TL. Water (hydrogen) in the lunar mantle: Results from petrology and magma ocean modeling. *Earth and Planetary Science Letters* 2011, **307**(1)**:** 173-179.
47. Saal AE, Hauri EH, Langmuir CH, Perfit MR. Vapour undersaturation in primitive mid-ocean-ridge basalt and the volatile content of Earth's upper mantle. *Nature* 2002, **419**(6906)**:** 451-455.
48. Fei Y, Ricolleau A, Frank M, Mibe K, Shen G, Prakapenka V. Toward an internally consistent pressure scale. *Proceedings of the National Academy of Sciences* 2007, **104**(22)**:** 9182.
49. Akahama Y, Kawamura H. Diamond anvil Raman gauge in multimegabar pressure range. *High Pressure Research* 2007, **27**(4)**:** 473-482.

Tables

Table 1 (A) Indexed powder XRD peaks of the H1-phase at 79 GPa and after *T* quench from 2100 K (Run# Sa083). The unit-cell parameters were obtained from powder XRD with *a*=10.021(2) Å and *c*=2.6121(9) Å. The X-ray wavelength was 0.3445 Å. (B) The atomic parameters of the H1-phase with space group of P63/m. A total of 774 reflections and 174 independent reflections from three merged grains were used for the structure determination and refinement, with wR2 = 13.35%, Goodness of fit on F^2= 1.151, and R1 = 5.59% for all data.

A	*hkl*	2ϑ-obs, °	*d*-obs, Å	*d*-calc, Å	*d*-diff, Å
	010	2.277	8.6692	8.6789	-0.0097
	020	4.545	4.3440	4.3395	0.0046
	120	6.018	3.2814	3.2803	0.0011
	030	6.824	2.8942	2.8930	0.0012
	220*	7.897	2.5015	2.5054	-0.0039
	130*	8.196	2.4104	2.4071	0.0033
	111*	8.528	2.3167	2.3163	0.0004
	021*	8.833	2.2368	2.2379	-0.0011
	040	9.122	2.1661	2.1697	-0.0036
	121*	9.673	2.0430	2.0434	-0.0004
	031*	10.193	1.9390	1.9387	0.0003
	131*	11.170	1.7699	1.7701	-0.0002
	221	10.935	1.8078	1.8081	-0.0003
	330	11.834	1.6709	1.6703	0.0007
	231	12.487	1.5839	1.5835	0.0004
	141*	12.895	1.5339	1.5333	0.0007

* Strong peaks in the powder XRD patterns.

B	Atom	S.O.F.	x/a	y/b	z/c
	Fe01		0.74451(17)	0.05948(16)	0.75
	Fe02		0.83694(14)	0.38349(13)	0.25
	Fe00	0.381	1.0	0	1.0
	O3		0.7161(7)	0.2257(7)	0.75
	O1		0.5949(7)	-0.0103(7)	0.25
	O2		0.7522(8)	-0.1146(8)	0.75

Table 2 Chemical compositions of the H1-phase in the run products.

Starting materials	MASFH30 (Run# Sb335)	MASFH6 (Run# Sb307)	$Al_{0.2}Fe_{0.8}(OH)_3$ (run# Sb343a)
P-T conditions	78 GPa 2000 K	96 GPa 2300 K	80 GPa 2100 K
Mg (at.%)	8.5(1.7)	4.9 (1.3)	
Si (at.%)	11.2(1.8)	12.6 (3.9)	
Al (at.%)	1.4(0.9)	11.2 (2.6)	1.5 (0.3)
Fe (at.%)	78.9(2.4)	71.3 (5.9)	98.5 (0.3)

Figures

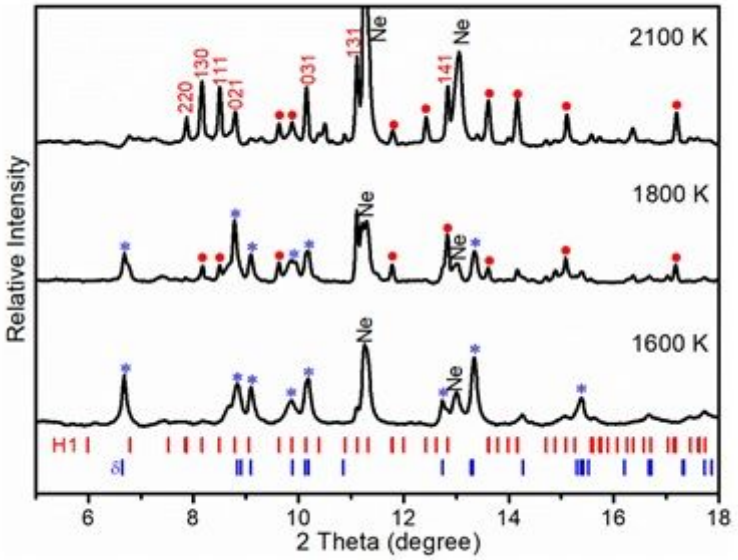

Figure 1

In-situ XRD observation of decomposition of δ-(Fe,Al)OOH into the H1-phase and Al-rich δ-phase at 79 GPa and 1600-2100 K. The starting material was (Fe0.8Al0.2)(OH)3 (Run# Sa083). A pure δ-phase was synthesized at 1600 K with a=4.436(1) Å, b=3.997(2) Å, c=2.587(1) Å, V=45.88(3) Å3; the H1-phase appeared at the expense of the δ-phase at 1800 K with a=10.075(4) Å, c=2.624(1) Å and V=230.7(2) Å3. The H1-phase becomes dominant at 2100 K with a=10.071(4) Å, c=2.622(1) Å and V=230.3(2) Å3. The peaks from the H1-phase and δ-phase are marked by red dots and blue asterisks, respectively. The calculated peak positions are indicated by small ticks. The X-ray wavelength was 0.3445 Å.

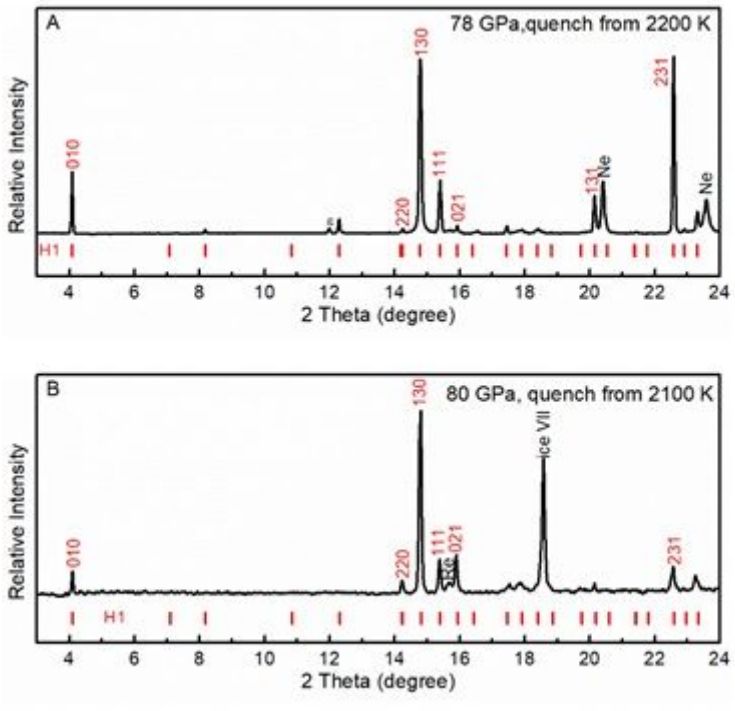

Figure 2

Synthesis of the H1-phase in the Fe2O3-H2O and FeO-H2O systems. (A) The H1-phase was synthesized in the starting material of Fe(OH)3 (Run# Sb343b). The H1-phase remained stable after heating at 2200K for 10 minutes with a=10.014(2) Å, c=2.6158(6) Å and V=227.18(7) Å3. (B) The H1-phase coexisting with ice-VII in the starting material of FeO+H2O at 80 GPa and T quench from 2100 K (Run# Sb390) with a=10.009(2) Å, c=2.6087(7) Å and V=226.3(1) Å3. The X-ray wavelength was 0.6199 Å.

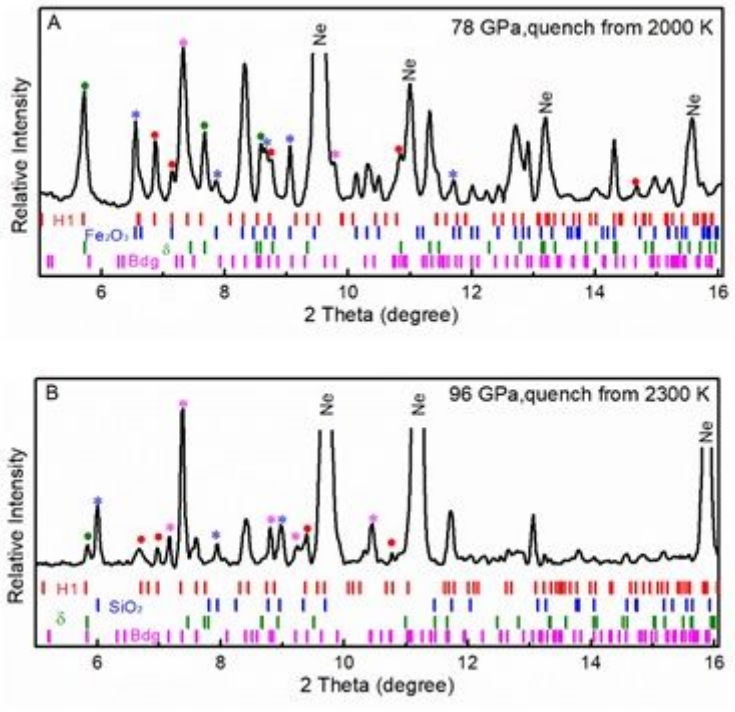

Figure 3

XRD patterns of the run products in Mg-Si-Al-Fe-O-H systems under high P-T conditions of the deep lower mantle. (A) The starting material was MASFH30 where the H1-phase coexisted with the pPv- Fe2O3, δ-phase, and bridgmanite. (B) The starting material was MASFH6 where the H1-phase coexisted with the CaCl2-type SiO2, δ-phase, and bridgmanite. The unit-cell parameters of each phase in the assemblage were obtained applying multigrain XRD (Table S2). The X-ray wavelength was 0.2905 Å.

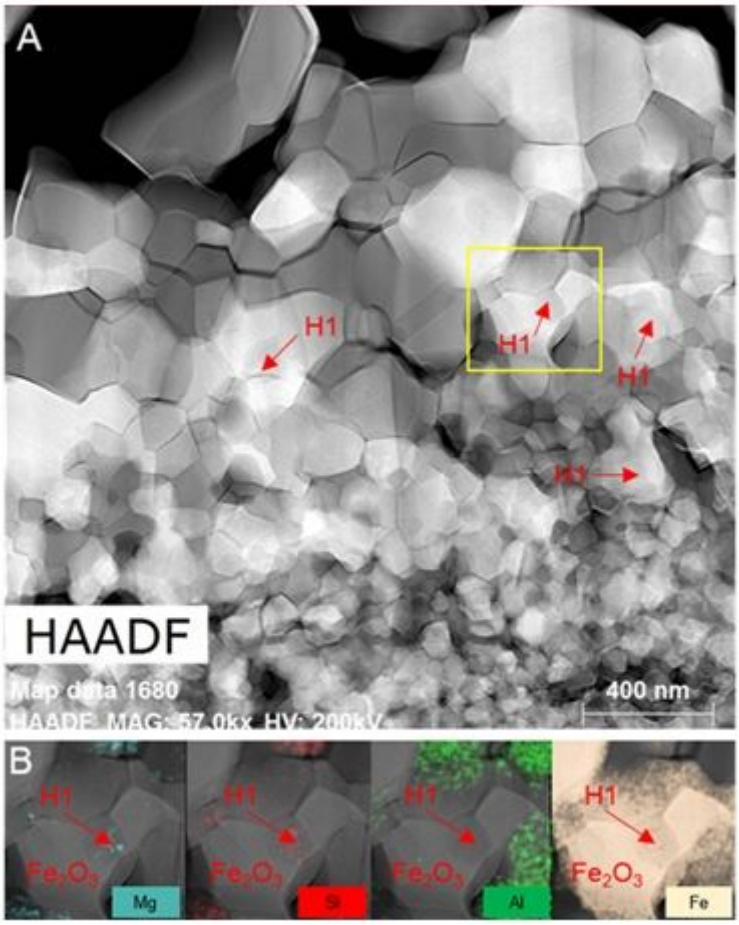

Figure 4

TEM image of the run product recovered from 78 GPa and 2000 K showing the presence of the H1-phase (Run# Sb335). The starting material was 40 mol% MgSiO3-30 mol% Al2O3-30 mol% Fe2O3. (A) Four grains of H1-phase were identified in the run product. (B) Elemental mapping of the selected area in (A). In contrast to the neighbouring pPv-Fe2O3 grain, the H1-phase contains considerable amounts of MgO and SiO2. Elemental mapping of Mg, Si, Al and Fe are shown in blue, red, green, and yellow, respectively.

Supplementary Files

This is a list of supplementary files associated with this preprint. Click to download.

- H1phase.cif
- SI1.docx